# On the Value of a Multistage Optimization Approach for Intensity-Modulated Radiation Therapy Planning*

D. Wood[1], S. Çetinkaya[†1,2], H. Gangammanavar[1], W. Lu[3], and J. Wang[3]

[1]Department of Operations Research and Engineering Management, SMU, Dallas, TX.
[2]Department of Internal Medicine, UTSW Medical Center, Dallas, TX.
[3]Department of Radiation Oncology, UTSW Medical Center, Dallas, TX.

Submitted to *Physics in Medicine and Biology*, February 3, 2022
Revised, May 26, 2022
Accepted, June 16, 2022

**Abstract**

Objective: Intensity-modulated radiation therapy (IMRT) aims to distribute a prescribed dose of radiation to cancerous tumors while sparing the surrounding healthy tissue. A typical approach to IMRT planning uniformly divides and allocates the same dose prescription across several successive treatment sessions. A more flexible fractionation scheme would lend the capability to vary dose prescriptions and utilize updated CT scans and future predictions to adjust treatment delivery. Therefore, our objective is to develop optimization-based models and methodologies that take advantage of adapting treatment decisions across fractions by utilizing predictions of tumor evolution.

Approach: We introduce a nonuniform generalization of the uniform allocation scheme that does not automatically assume equal dose prescriptions for all sessions. We develop new deterministic and stochastic multistage optimization-based models for such a generalization. Our models allow us to simultaneously identify optimal dose prescriptions and fluence maps for individual sessions. We conduct extensive numerical experiments to compare these models using multiple metrics and dose-volume histograms.

Main results: Our numerical results in both deterministic and stochastic settings reveal the restrictive nature of the uniform allocation scheme. The results also demonstrate the value of nonuniform multistage models across multiple performance metrics. The improvements can be maintained even when restricting the underlying fractionation scheme to small degrees of nonuniformity.

Significance: Our models and computational results support multistage stochastic programming methodology to derive ideal allocation schemes and fluence maps simultaneously. With technological and computational advancements, we expect the multistage stochastic programming methodologies to continue to serve as innovative optimization tools for radiation therapy planning applications.

*This work has been conducted under a Lyle School (SMU) Interdisciplinary Research Seed Funding Grant and Radiation Oncology MAIA Lab (UTSW) Educational Experience Agreement (UTSW Contract ID # 2020-7031).
[†]Corresponding author: sila@smu.edu

# 1 Introduction and Relevant Literature

Radiation therapy is a standard treatment method for various forms of cancer, and it involves meticulously exposing the impacted tissues to radiation to kill the malignant tumor cells. For successful treatment outcomes, it is vital to deliver the prescribed radiation dose to the tumor while minimizing exposure to healthy organs-at-risk (OAR) (Pardalos & Romeijn 2009, Holder & Salter 2005). The common scheduling practice for radiation therapy treatment includes multiple successive sessions (*fractions*) regularly occurring over several weeks. This fragmented scheduling approach is known as a *fractionation scheme*. A fractionation scheme is advantageous because healthy cells can effectively repair sub-lethal damage between fractions, whereas the tumor cells are much less capable (Baskar et al. 2012). As clinical imaging, delivery technologies, and computational capabilities have improved, there has been a continual need to study and improve the existing optimization-based radiation therapy planning (RTP) practices and approaches. This paper revisits this need with a specific focus on Intensity-Modulated Radiation Therapy (IMRT), an advanced technology known to produce a precise and conformal radiation dosage delivery by utilizing numerous beamlets with varying intensities.

Since its first clinical implementation in 1994, IMRT has resulted in significant reductions in radiation exposure to healthy tissues for patients undergoing treatment (Mills & Woo 2015, Teh et al. 1999). Effective delivery of IMRT relies on optimization-based RTP models and methodologies to obtain an optimal fluence map (FM), a.k.a., beamlet intensity profile. The FM is determined while considering the state of the patient (volume of the tumor and its position relative to OARs as seen on volumetric imaging such as a CT scan) and the tumor prescription provided by a clinician (Bortfeld 1999, 2006, Brahme et al. 1982, Ehrgott et al. 2010, Redpath et al. 1976, McDonald & Rubin 1977, Mell et al. 2003, Shepard et al. 1999, Starkschall 1984, Webb 2003). For detailed reviews of optimization-based approaches for IMRT, we refer to Bortfeld (1999), Ehrgott et al. (2010), Shepard et al. (1999). Here we review previous work most closely related to our work.

A popular optimization-based approach for determining the optimal FM is through the implementation of RTP models with a least-squares objective function. RTP models that incorporate a least-squares objective function date back several decades (Redpath et al. 1976, McDonald & Rubin 1977, Starkschall 1984). We refer to Section 2.3.1 of Ehrgott et al. (2010) for a review of this class of RTP optimization models. In the context of an RTP problem, a least-squares objective penalizes any deviation between the given prescription and the radiation quantities delivered to the tumor. The resulting model will also typically include upper bound constraints on the amount of radiation exposure to surrounding OAR. Such current least-squares models determine the FM while only considering the patient's state at the beginning of radiation therapy, and the same FM is adopted for radiation delivery for all fractions that follow (Romeijn & Dempsey 2008, Men et al. 2012). We classify such an approach to RTP as the *static approach*.

The static approach assumes that the tumor prescription quantity and OAR upper bounds remain fixed and uniform across all fractions. We refer to this kind of a dose prescription allocation scheme as *uniform fractionation* in the remainder of this paper. However, with treatment lasting several weeks, the tumor and OAR structures are expected to reveal consistent **evolution** in volume between fractions (Lu et al. 2008, Ferris & Voelker 2004, Ramakrishnan et al. 2012). A more flexible fractionation scheme would lend capability and perhaps allow the clinician to utilize updated CT scans or future predictions during the treatment process to make adjustments to treatment delivery. Therefore, there is a need to develop optimization-based models and methodologies that take advantage of this capability.

To this end, we propose RTP models and methodology that explicitly adopt the FM at each fraction following a patient's predicted structural volume evolution over time. In contrast to the existing static approach with uniform fractionation, we have a multistage approach to *nonuniform fractionation*. A CT scan provides essential information only at the current point in time. However, the radiation delivered in a given fraction impacts the future evolution of the tumor and surrounding structures. Hence, our proposed multistage approach with a nonuniform fractionation scheme is more amenable to incorporate **uncertainty in regards to evolution**

**of the tumor and OAR over future fractions** (a.k.a., *interfractional uncertainty* (Men et al. 2012)) and adapt FMs in response to uncertainty.

Our paper aims to enhance and inform the existing optimization-based practice for RTP to include a stochastic multistage framework. Hence, we systematically examine the potential shortcomings of the static approach compared to the proposed multistage approach. To this end, we explore the value of a nonuniform fractionation scheme and illustrate that allowing the dose prescriptions to vary across fractions may have quantifiable advantages worthy of evaluation by clinical experts. First, we assume a deterministic setting (with perfect tumor evolution predictions for each fraction). We offer computational results using prostate cancer patient CT scan data and compare various metrics of interest and resulting dose-volume histograms (DVHs). We also provide insights from models that restrict the degree of nonuniformity in the fractionation scheme.

Next, we consider the more realistic stochastic case with interfractional uncertainty. For this purpose, we utilize the multistage stochastic programming (SP) modeling approach. This approach relies upon a scenario tree representation where each tree node represents a prediction of the future state of the tumor. Stochastic programming is a practical framework for large-scale decision-making under uncertainty. We refer the reader to Birge & Louveaux (2011), Shapiro et al. (2014) for a comprehensive introduction to stochastic programming modeling approaches and solution methods. Stochastic programming has proven very effective in various application domains, including healthcare (see Wallace & Ziemba (2005) for a survey). Building upon these, our approach enables seamless integration of predictive analytics tools for decision-making for RTP. Thereby, we make a case in support of employing multistage stochastic programming methodology to simultaneously derive ideal allocation schemes and FM solutions, in contrast to the common practice static approach.

The rest of the paper is organized as follows. In Section 2, we present the notation and foundational elements of the optimization-based RTP models investigated in the paper. We also present the main performance metrics used to compare the different approaches for RTP.

In Section 3, we consider a deterministic multistage model that serves as a building block for the stochastic multistage models. We also demonstrate the value of our proposed nonuniform fractionation scheme. In Section 4, we extend the deterministic case to take into account interfractional uncertainty explicitly. Next, in Section 4.3, we provide a comparative analysis of the performance and demonstrate the potential benefits of the stochastic multistage models in a three-stage RTP experiment. Finally, we present a summary of our results and conclusions in Section 5.

# 2 Fundamentals of Optimization-Based Modeling for RTP

We begin by introducing fundamental notions of the optimization-based IMRT planning problems at hand, along with the corresponding notation adopted throughout this paper. In terms of the notation, let us first note that we use boldface lowercase letters when referring to a vector (e.g., $\mathbf{z}_n$), boldface uppercase letters for a matrix (e.g., $\mathbf{A}_n$), and calligraphic uppercase letters (e.g., $\mathcal{O}$) for sets. Also, we reserve the assignment of subscripts for the purposes of time or stage indices, and we note that $[a]_+ := \max\{a, 0\}$ and $[a]_- := \max\{-a, 0\}$ for $a \in \mathbb{R}$. For a summary of all necessary notations used throughout this paper, we refer to Appendix A.

## 2.1 Problem Definition, Modeling Assumptions, and Notation

Suppose we have a fractionation scheme comprising of $N$ fractions. At the beginning of any fraction, we have the ability to obtain a CT scan which captures a 3D representation of the patient's current state (structural volumes and positions) and includes all relevant structures such as the tumor, the nearby OARs, and normal body tissue. We collectively denote these structures by $\mathcal{T}$. Depending on the type and location of cancer, the set of OAR, denoted as $\mathcal{O} \subset \mathcal{T}$, is different. For example, the CT scan of a prostate cancer patient may have an OAR set given by $\mathcal{O} := \{\text{rectum, bladder, left femur, right femur}\}$.

We emphasize the idea that each CT scan represents an instantaneous observation of the patient's state (denoted $\xi_n$ in fraction $n$) and can be viewed as a realization of a stochastic process

$\{\tilde{\xi}\}$ associated with the evolution of a patient's structures. For clarity, a distinction is made when a particular CT scan observation is currently known ($\xi_n$) (has already been realized/obtained) or currently unknown ($\tilde{\xi}_n$) (to be revealed in the future). The information in a CT scan is discretized into a three-dimensional grid, where the smallest unit is called a *voxel*. Based on its relative position, a voxel ($v$) is classified as belonging to a specific structure $i \in \mathcal{T}$. We use $\mathcal{V}_n^{(i)}$ to represent the set of voxels in a particular fraction $n$ classified to structure $i \in \mathcal{T}$. We define the set of all voxels as $\mathcal{V}_n := \bigcup_{i \in \mathcal{T}} \mathcal{V}_n^{(i)}$.

The fractionation scheme takes the *dose prescription* as an input which dictates the total quantity of radiation (in Gray (Gy) units) assigned for delivery to the patient's tumor ($L^{\text{tumor}}$) across all $N$ fractions. The does prescription also dictates structure specific upper bounds, denoted by the vector $\mathbf{u}$, on the amount of radiation delivered to the surrounding OAR. The total quantity of radiation is distributed into fraction-specific prescription quantities captured by variables $\ell_n$ and $\mathbf{z}_n$ for tumor and OAR, respectively, in a given fraction $n$, respectively. That is, $\ell_n$ is the radiation amount assigned for delivery to the tumor whereas $\mathbf{z}_n$ is the upper bound on the amount of radiation delivered to OAR in fraction $n$. Therefore, the decision vector $(\mathbf{z}_n, \ell_n)$ specifies the fraction-specific dose prescriptions. Clearly, these variables must satisfy

$$\sum_{n=1}^{N} \ell_n = L^{\text{tumor}}, \tag{1a}$$

$$\sum_{n=1}^{N} z_n^{(i)} \leq u^{(i)}, \quad i \in \mathcal{O} \tag{1b}$$

where, Constraint (1a) represents the total dose prescription (DP) assigned to the tumor and Constraints (1b) represents the upper limit of the DP impacting each OAR $i \in \mathcal{O}$. That is, (1a) ensures that the sum of fraction-specific tumor dose prescriptions must be equal to the overall treatment dose prescription ($L^{\text{tumor}}$) whereas (1b) limits the total of the OAR upper bounds for each structure $i \in \mathcal{O}$ to be at most the prescribed value given in $\mathbf{u}$.

To model the requirements of a fractionation scheme (uniform or nonuniform), we introduce

a set of feasible fraction-specific dose prescriptions as

$$\mathcal{U}_n^{\epsilon} = \left\{ (\mathbf{z}_n, \ell_n) \;\middle|\; \begin{array}{ll} \dfrac{L^{\text{tumor}}}{N} \cdot (1-\epsilon) \leq \ell_n \leq \dfrac{L^{\text{tumor}}}{N} \cdot (1+\epsilon), & \text{(2a)} \\ \dfrac{u^{(i)}}{N} \cdot (1-\epsilon) \leq z_n^{(i)} \leq \dfrac{u^{(i)}}{N} \cdot (1+\epsilon), \quad i \in \mathcal{O}, . & \text{(2b)} \end{array} \right\}$$

Here, the parameter $\epsilon \geq 0$ determines the degree of nonuniformity allowed in choosing the fraction-specific prescription upper bounds. For instance, when $\epsilon = 0$, (2a) and (2b) imply a uniform fractionation scheme with tumor prescription $\ell_n = \frac{L^{\text{tumor}}}{N}$ and OAR upper bounds $z_n^{(i)} = \frac{u^{(i)}}{N}$ for structures $i \in \mathcal{O}$, for all fractions. On the other hand, we use $\mathcal{U}_n^M$ to imply a completely unrestricted nonuniform fractionation scheme, where $M$ is a large positive scalar.

In a given fraction denoted by $n$, where $n = 1, \ldots, N$, a multileaf collimator is used to precisely conform radiation delivery to the tumor structure (Holder & Salter 2005, Ehrgott et al. 2010, Ghate 2011). The radiation delivery involves determining the gantry angle (alignment of beams) and intensity of each individual beamlet. We denote the set of radiation beamlets as $\mathcal{B}$. We assume that the gantry angle is preselected and focus on determining the FM. For a given gantry angle and the information provided in a CT scan ($\xi_n$), a *dose-deposition matrix* that translates a given FM to the amount of radiation delivered to each individual voxel is computed. We denote the dose-deposition matrix in fraction $n$ by $\mathbf{A}_n(\xi_n)$ to explicitly show its dependence on the CT-scan information. An element $a_{vbn}$ of the dose-deposition matrix $\mathbf{A}_n(\xi_n)$ captures the amount of radiation from beamlet $b \in \mathcal{B}$ delivered to voxel $v \in \mathcal{V}$. We denote the amount of radiation delivered to voxel $v \in \mathcal{V}$ by $x_{vn}$. If $y_{bn}$ denotes the beamlet intensity for $b \in \mathcal{B}$, then we have $x_{vn} = \sum_{b \in \mathcal{B}} a_{vbn} y_{bn}$. This relationship can be written concisely as

$$\mathbf{x}_n = \mathbf{A}_n(\xi_n)\mathbf{y}_n \qquad \forall n = 1, \ldots, N. \tag{3}$$

The amount of radiation received by a OAR-classified voxel must be no more than the respective fraction-specific upper bound, that is

$$x_{vn} \leq z_n^{(i)} \qquad \forall v \in \mathcal{V}_n^{(i)},\ i \in \mathcal{O},\ n = 1, \ldots, N. \tag{4}$$

The optimization models presented in this paper simultaneously determine the distribution of the dose prescription into fraction-specific amounts and construct precise FMs for all fractions.

The vector $(\mathbf{x}_n, \mathbf{y}_n)$ collectively determines the FM. The set of feasible fraction-specific radiation delivery decisions is then given by

$$\mathcal{S}_n(\xi_n) = \big\{(\mathbf{x}_n, \mathbf{y}_n, \mathbf{z}_n, \ell_n) \mid (3), (4),\ \mathbf{x}_n, \mathbf{y}_n, \mathbf{z}_n, \ell_n \geq 0\big\},\ n = 1, \ldots, N. \tag{5}$$

As previously mentioned, a popular method for meeting tumor dose prescription is through the use of a fraction-specific least-squares expression for

$$f_n(\mathbf{x}_n, \ell_n) = \sum_{v \in \mathcal{V}_n^{\text{tumor}}} \left[ w_n^+ \Big( \Big[ x_{vn} - \ell_n \Big]_+ \Big)^2 + w_n^- \Big( \Big[ x_{vn} - \ell_n \Big]_- \Big)^2 \right],\ n = 1, \ldots, N. \tag{6}$$

Clearly, $f_n(\cdot)$ penalizes deviation between the quantity of radiation actually delivered to each voxel $(x_{vn})$ and the quantity prescribed in a given fraction $(\ell_n)$. In this sense, $f_n$ is a measure of radiation delivery precision to all tumor voxels in a particular fraction $(\mathcal{V}_n^{\text{tumor}})$. For all $n$, the scalar weight parameters $w_n^+ > 0$ and $w_n^- > 0$ used in (6) reflect the preferences between overdosing and underdosing the tumor, respectively. For example, choosing a value $w_n^- > w_n^+$ implies heavier penalization to underdosing the tumor as opposed to overdosing the tumor. Without loss of generality, we use $w_n^+ + w_n^- = 1$ for $n = 1, \ldots, N$ in our numerical experiments.

## 2.2 Performance Evaluation Metrics

We next present the metrics useful to compare the performance of different optimization-based approaches of interest in this paper. These include the squared deviation penalty (SDP), overall total dose (TD-Overall), OAR total dose (TD-OAR), and tumor underdose (TUD). These metrics are computed as

$$\text{SDP} = \sum_{n=1}^{N} f_n(\mathbf{x}_n, \ell_n), \qquad \text{TUD} = \frac{1}{N} \sum_{n=1}^{N} \frac{100 \times |\{v \in \mathcal{V}_n^{\text{tumor}} : x_{vn} < \ell_n\}|}{|\mathcal{V}_n^{\text{tumor}}|},$$

$$\text{TD-Overall} = \frac{\sum_{n=1}^{N} \sum_{i \in \mathcal{T}} \sum_{v \in \mathcal{V}_n^{(i)}} x_{vn}}{\sum_{n=1}^{N} \sum_{i \in \mathcal{T}} |\mathcal{V}_n^{(i)}|}, \qquad \text{and} \qquad \text{TD-OAR} = \frac{\sum_{n=1}^{N} \sum_{i \in \mathcal{O}} \sum_{v \in \mathcal{V}_n^{(i)}} x_{vn}}{\sum_{n=1}^{N} \sum_{i \in \mathcal{O}} |\mathcal{V}_n^{(i)}|},$$

where $f_n$ is given in (6). SDP captures the total quadratic penalty on radiation delivery deviating from the dose prescription $(\ell_n)_{n=1}^N$. TD-Overall represents the average amount of radiation

delivered to all voxels through the entire treatment horizon. This metric includes dosage delivered to all OAR, the tumor, and normal tissue. On the other hand, TD-OAR corresponds to the average amount of radiation delivered only to OAR voxels through the entire treatment horizon. TUD calculates the average percentage of tumor voxels that receive less than the prescribed amount of radiation. In addition to the metrics of interest above, we also define the notion of aggregate dose (AD) that represents the total amount of radiation delivered to all voxels through the entire treatment horizon. We compute this quantity as $\text{AD} = \sum_{n=1}^{N} \sum_{i \in \mathcal{T}} \sum_{v \in \mathcal{V}_n^{(i)}} x_{vn}$. We make references to this quantity whenever appropriate.

It is worthwhile to note that while the above metrics are fundamental for optimization-based approaches, they are not routinely evaluated for a clinical plan. The existing clinical routine evaluates a plan using DVHs (Pardalos & Romeijn 2009, Drzymala et al. 1991). Hence, we also present the comparison of our proposed models using DVHs.

### 2.3 Basic Model of the Static Approach

As we have noted earlier, standard practice for solving RTP problems is based on the static approach under which the treatment plan is designed and based only on the information $\xi_1$ revealed in the CT scan obtained before the commencement of the treatment. These approaches provide a lucid comparative setting for our proposed multistage approach and nonuniform fractionation scheme. Such a comparison will enable us to demonstrate the advantages of the proposed methods for potential consideration in practice. For this reason, before we introduce our proposed models in the next section, we present the underlying basic model of the static approach that ignores the uncertain evolution of the tumor and OAR over future fractions.

We refer to this model as the static model and denoted by (**S**) below. The model determines an optimal FM that minimizes the fraction-specific squared deviation penalty subject to the

requirements of a uniform fractionation scheme. It is formulated as

$$\min \ f_1(\mathbf{x}_1, \ell_1) \tag{S}$$
$$\text{subject to } (\mathbf{x}_1, \mathbf{y}_1, \mathbf{z}_1, \ell_1) \in \mathcal{S}_1(\xi_1) \cap \mathcal{U}_1^0,$$

and implemented in a static fashion. Let $(\mathbf{x}_1^\star, \mathbf{y}_1^\star)$ denote the optimal FM obtained by solving the static model (**S**). Under the static approach, the same FM $(\mathbf{x}_1^\star, \mathbf{y}_1^\star)$ is used in every fraction going forward (i.e., for fractions $n = 2, \ldots, N$). Since the optimization model only uses information available at the beginning of the treatment and does not consider any future prediction, (**S**) can be classified as a single-stage model (in contrast to the multistage models proposed in this paper). As mentioned in Saberian et al. (2017), this model is representative of and analogous with what is utilized in practice.

As expected, the optimal FM $(\mathbf{x}_1^\star, \mathbf{y}_1^\star)$ computed based on the static model (**S**) is likely to be suboptimal for future fractions $n = 2, \ldots, N$ when the tumor and OAR may have evolved. Such suboptimality may result in undesirable ramifications, as will be illustrated in our computational experiments. The fractionation scheme lends itself to obtaining new CT scans during a course of treatment. The adaptive radiation therapy (ART) approach takes advantage of this ability and involves occasional replanning with newer CT images (Yan et al. 1997). Therefore, ART involves solving a sequence of static problems of the form in (**S**). ART is commonly applied in clinical practice when the tumor is expected (or observed) to grow or shrink. Supplemental methods have been developed to detect interfractional patient anatomy changes and effectively replan in order to maintain conformality. For example, deformable image registration can be employed to determine voxel correspondance and positional transformations among a set of scans (Oh & Kim 2017). Another approach involves in-room CT for direct replanning as this allows for imaging and reoptimization to take place immediately before the fractional dose is delivered (Ahunbay et al. 2008). Since the current practice of ART and the alternative approaches mentioned above involve static models, we cannot incorporate predictions on future anatomical changes. The multistage models that we describe next are intended to address these shortcomings of the static approach in a fractionated setting.

# 3 Deterministic Multistage Formulations

A deterministic multistage setting is suitable when the patient's current condition is known (from the latest CT scan) and a prediction for each subsequent fraction (one prediction for each future fraction) is available from the beginning of the treatment. Such future predictions are also known as the *lookahead information*. The predictions are available in the form of a sequence of predicted CT scans $\{\xi_n\}_{n=2}^N$ (note that $\xi_1$ is already known from the initial CT scan). We highlight the distinction between having a single-point prediction for each future fraction (deterministic) rather than multiple predictions in the form of scenarios with different probabilities at each fraction (stochastic).

Using the CT-scan information, the dose-deposition matrices $\mathbf{A}_n(\xi_n)$ are computed for $n = 1, \ldots, N$. Since the deterministic multistage models accommodate structural evolution through CT-scan information $\{\xi_n\}_{n=1}^N$, they are able to provide FMs that are tailored to this information. From a clinical perspective, this is a hypothetical setting (unless, predictive methods are used proactively); yet, the setting provides a foundation for academic research which incorporates future predictions (perfect or otherwise) and sets the stage for a more general stochastic setting that accommodates multiple predicted scenarios.

## 3.1 Uniform Deterministic Multistage Model

The static model (**S**) discussed in the previous section relies on the most basic implementation of the uniform fractionation scheme by completely ignoring the evolution of the tumor and OAR over future fractions. This fractionation scheme may also be implemented in the context of the deterministic multistage setting. This leads us to the following model that we refer to as the uniform deterministic multistage model and denoted by (**UD**):

$$\begin{aligned} \min \ & \sum_{n=1}^{N} f_n(\mathbf{x}_n, \ell_n) \\ \text{subject to } & (\mathbf{x}_n, \mathbf{y}_n, \mathbf{z}_n, \ell_n) \in \mathcal{S}_n(\xi_n) \cap \mathcal{U}_n^0, \quad \forall n = 1, \ldots, N. \end{aligned} \tag{\textbf{UD}}$$

Notice that the fraction-specific dose prescription decisions must satisfy $(\ell_n, \mathbf{z}_n) \in \mathcal{U}_n^0$ that enforces the requirements for the uniform fractionation scheme. The fraction-specific decisions must additionally belong to the set $\mathcal{S}_n(\xi_n)$. The model aims to minimize the SDP computed across all $N$ fractions.

It is worthwhile to note that, due to the uniform fractionation scheme, the fraction-specific dose prescriptions of the uniform deterministic multistage model (**UD**) must be trivially set to $\ell_n = \frac{L^{\text{tumor}}}{N}$ and $z_n^{(i)} = \frac{u^{(i)}}{N}$, the constraints (1) are rendered redundant, and the formulation decomposes by fractions reducing the model to

$$\sum_{n=1}^{N} \Big( \min \ \big\{ f_n\big(\mathbf{x}_n, \ell_n\big) \ \big| \ (\mathbf{x}_n, \mathbf{y}_n, \mathbf{z}_n, \ell_n) \in \mathcal{S}_n(\xi_n) \cap \mathcal{U}_n^0 \big\} \Big). \tag{7}$$

The above observation implies that there is no value in incorporating the lookahead information in RTP under uniform fractionation scheme. In other words, the uniform fractionation scheme does not lend the optimization model enough freedom to take advantage of the lookahead knowledge. Hence, there is a strong motivation to explore less restrictive multistage models capable of effectively utilizing predicted tumor evolution information in the fractionated setting. This leads us to the nonuniform multistage models that we discuss next.

### 3.2 Nonuniform Deterministic Multistage Model

To model the nonuniform fractionation scheme, we relax the restrictions on the fraction-specific dose prescriptions. We achieve this by introducing $\epsilon > 0$ which expands the set of feasible fraction-specific dose prescriptions $\mathcal{U}_n^\epsilon$. Moreover, in relation to the feasible sets used in (**UD**), the sets of feasible fraction-specific dose prescriptions now satisfy $\mathcal{U}_n^\epsilon \supset \mathcal{U}_n^0$ for $n = 1, \ldots, N$. The resulting optimization model under nonuniform fractionation is then given by

$$\begin{aligned} \min \ & \sum_{n=1}^{N} f_n(\mathbf{x}_n, \ell_n) \\ \text{subject to } & (1); \ (\mathbf{x}_n, \mathbf{y}_n, \mathbf{z}_n, \ell_n) \in \mathcal{S}_n(\xi_n) \cap \mathcal{U}_n^\epsilon, \quad \forall n = 1, \ldots, N. \end{aligned} \tag{ND}$$

Notice that in the above model, the dose-prescription decision variables ($\mathbf{z}_n$, $\ell_n$) are no longer trivially determined for every fraction. Therefore, the fraction-specific dose prescriptions ($\mathbf{z}_n$,

$\ell_n$) as well as the FMs $(\mathbf{x}_n, \mathbf{y}_n)$ are adaptive in response to the future lookahead information.

A couple of observations regarding (**ND**) are in order. Firstly, as a consequence of $\mathcal{U}^\epsilon \supset \mathcal{U}_n^0$, for any fraction $n$, we have $\{\mathcal{S}_n(\xi_n) \cap \mathcal{U}_n^\epsilon\} \supseteq \{\mathcal{S}_n(\xi_n) \cap \mathcal{U}_n^0\}$. Therefore, it is evident that the optimal objective function value of the nonuniform deterministic multistage model (**ND**) is at most the optimal objective function value of (**UD**). Secondly, it is worthwhile to mention that ($\mathbf{z}_n$, $\ell_n$) are coupled across fractions through constraints (1). Therefore, unlike (**UD**), the formulation of (**ND**) does not decompose by fractions.

Observe that neither of the deterministic multistage models ((**UD**) and (**ND**)) take total dose (Overall or OAR) into consideration explicitly. From a practical point of view, a precise delivery plan is desirable. However, if this precise delivery comes at the cost of relatively higher TD-Overall and TD-OAR, implying greater exposure for the patient, then such a plan is not ideal. To address this issue, we revise the nonuniform deterministic multistage model (**ND**) as

$$\begin{aligned} \min \ & \sum_{n=1}^{N} f_n(\mathbf{x}_n, \ell_n) && \text{(RND)} \\ \text{subject to } & (1);\ (\mathbf{x}_n, \mathbf{y}_n, \mathbf{z}_n, \ell_n) \in \mathcal{S}_n(\xi_n) \cap \mathcal{U}_n^\epsilon, \quad \forall n = 1, \ldots, N, \\ & \sum_{n=1}^{N} \sum_{i \in \mathcal{T}} \sum_{v \in \mathcal{V}_n^{(i)}} x_{vn} \leq \bar{\tau}. && (8) \end{aligned}$$

The additional constraint (8) in the model bounds the feasible AD quantity by a given upper bound $\bar{\tau} \in \mathbb{R}_+$. Specifically, if we set $\bar{\tau} = \sum_{n=1}^{N} \sum_{i \in \mathcal{T}} \sum_{v \in \mathcal{V}_n^{(i)}} x_{vn}^{\star UD}$, then the AD prescribed by (**RND**) is bounded above by the optimal AD under (**UD**).

It is not guaranteed that the (**UD**) results in a lower total dose when compared to (**ND**). But when it does, then the second constraint in the revised model is active. However, since the revised model uses the optimal solution (**UD**), the additional constraint results in added computational expense resulting from solving two optimization problems. Procedure 1 summarizes how to make use of the proposed multistage models presented so far.

**Procedure 1** Nonuniform Deterministic Fractionation Procedure.

1: **Input:** Number of fractions, $N$; total dose prescription $\mathbf{u}$ and $L^{\text{tumor}}$; current CT-scan information $\xi_1$ and a prediction of structural evolution $\{\xi_n\}_{n=2}^{N}$.

2: Compute the dose-deposition matrices $\mathbf{A}_n$ for $n = 1, \ldots, N$.

3: Solve the uniform deterministic model (**UD**) and obtain the optimal solution $\mathbf{x}_n^{\star UD}$ for $n = 1, \ldots, N$. Using the optimal solution, compute AD for (**UD**).

4: Using AD from (**UD**) as $\bar{\tau}$, instantiate and solve the revised nonuniform model (**RND**). Obtain the optimal solution $(\mathbf{x}_1^\star, \mathbf{y}_1^\star, \mathbf{z}_1^\star, \ell_1^\star)$.

5: **Output:** The optimal dose prescriptions $(\mathbf{z}_1^\star, \ell_1^\star)$ and the beamlet intensities $\mathbf{y}_1^\star$.

### 3.3 Numerical Results for a Comparison of the Deterministic Models

We now turn our attention to the numerical evaluation of the deterministic multistage models presented so far, viz., (**S**), (**UD**), (**ND**), and (**RND**). Our first objective is to establish the relative performance for each of the four models in terms of SDP, TD-Overall, TD-OAR, and TUD, as defined in Section 2.2. Our second objective is to demonstrate the superiority of the (**RND**) with respect to all metrics of interest. To this end, we utilize a prostate cancer CT scan dataset in the form of dose-deposition matrices provided by Saberian et al. (2016). This dataset is available online (http://faculty.washington .edu/archis/spintfracdata.zip) and it does not include the actual CT scans. That is, the dataset basically provides five collections of structure-specific dose-deposition matrices corresponding to five unique prostate CT scans. For the numerical experiments regarding our deterministic multistage models, we choose three of the five provided collections (dose-deposition matrices) that reasonably represent a prostate cancer patient's structural evolution over $N = 3$ fractions. The underlying scans may reveal differences among each other in terms of the volumetric sizes of the tumor and OAR and, resultingly, the relative positions of all structures. For example, a patient's bladder may reveal an increase or decrease in volume from one fraction to the next. Specifically, the OAR structures considered are the rectum, bladder, and the left and right femoral heads.

We preprocess[1] all dose-deposition matrices to suit our experimental setting and objectives. These three scans (labeled as Scan 1, Scan 3, and Scan 4 in our data files), in turn, are used to generate six ($3! = 6$) scan sequences illustrated in Table 1.

| Scan Sequences | First-Stage | Second-Stage | Third-Stage |
|---|---|---|---|
| 1 | Scan 1 | Scan 4 | Scan 3 |
| 2 | Scan 1 | Scan 3 | Scan 4 |
| 3 | Scan 3 | Scan 1 | Scan 4 |
| 4 | Scan 3 | Scan 4 | Scan 1 |
| 5 | Scan 4 | Scan 1 | Scan 3 |
| 6 | Scan 4 | Scan 3 | Scan 1 |

Table 1: Scan Sequences Used to Generate Numerical Instances for Deterministic Models.

We assume that the differences between the scans represent a patient's physical structures evolving between fractions. We use two sets of parameters denoted by $P1$ and $P2$ that are summarized in Table 2 and differ in the values for weights $(w_n^+, w_n^-)$. The parameter set $P1$ penalizes tumor underdose and overdose equally (i.e., $w_n^+ = w_n^- \ \forall n$) whereas $P2$ heavily penalizes under dosage of the tumor (i.e., $w_n^+ \ll w_n^- \ \forall n$). When combined with the scan sequences summarized in Table 1, parameter sets $P1$ and $P2$ result in a total of twelve instances, (i.e., six instances each for $P1$ and $P2$, respectively) of the deterministic multistage models.

| Set | N | $L^{\text{tumor}}$ | $u^{\text{rectum}}$ | $u^{\text{bladder}}$ | $u^{\text{left femur}}$ | $u^{\text{right femur}}$ | $w^+$ | $w^-$ |
|---|---|---|---|---|---|---|---|---|
| $P1$ | 3 | 81 | 75 | 79 | 55 | 55 | 0.5 | 0.5 |
| $P2$ | 3 | 81 | 75 | 79 | 55 | 55 | 0.001 | 0.999 |

Table 2: Parameter Sets $P1$ and $P2$.

### 3.3.1 Impact of Nonuniform Fractionation on the Metrics of Interest and DVHs

For the first set of experiments, we consider the most general (relaxed) versions of the nonuniform deterministic multistage models obtained by using $\epsilon = M$ in the description of the set $\mathcal{U}_n^\epsilon$ (see (1)). In Table 3, we report the resulting average values of metrics SDP, TD-Overall, TD-OAR, and TUD, computed over all numerical instances under $P1$ (six scan sequences) and $P2$ (six scan sequences), for each model. Also, although TUD is computed for each fraction individually, the average performance over the $N = 3$ fractions is reported.

[1]For the purposes of numerical results presented in this paper, all dose-deposition matrix instances were obtained from Saberian et al. (2016) and were generated by the authors' in-house phantom creator software PhanC written in MATLAB (Saberian & Kim 2014).

| | Parameter Set $P1$ | | | | Parameter Set $P2$ | | | |
|---|---|---|---|---|---|---|---|---|
| | SDP | TD-Overall | TD-OAR | TUD | SDP | TD-Overall | TD-OAR | TUD |
| (**S**) | 184420.0128 | 4.2247 | 8.8811 | 50.5555 | 283651.5815 | 4.0502 | 8.0958 | 36.5689 |
| (**UD**) | 358.6021 | 4.2375 | 8.2729 | 48.7630 | 196.0174 | 4.0727 | 6.7470 | 3.1840 |
| (**ND**) | 220.2699 | 4.6349 | 8.6301 | 48.3648 | 3.9990 | 4.2457 | 7.6717 | 9.0562 |
| (**RND**) | 222.3800 | 4.2375 | 7.9658 | 48.4390 | 6.6025 | 4.0715 | 6.1853 | 1.2108 |

Table 3: A Comparison of Metrics of Interest for Deterministic Models under Parameter Sets $P1$ and $P2$: Comprehensive Numerical Results Reporting Average Values over All Numerical Instances.

The results indicate the severe inadequacy of the static approach across both parameter sets, in terms of SDP, TD-OAR, and TUD. This observation validates our idea that simply using the same FM for all fractions in a setting where patient structural evolution is present may lead to undesirable outcomes (increased exposure to OAR and reduced radiation precision). The multistage models that utilize the prediction information to adapt FMs across fractions address the shortcoming of the static approach. The improvement is most evident in the SDP results under both settings. The value of nonuniform fractionation is evident by comparing the SDP results of (**UD**) and (**ND**). Since both the models aim to minimize the SDP and (**UD**) imposes additional restrictions on how the overall prescription is distributed into fraction-specific prescriptions, the SDP is higher (62.8%) for (**UD**) when compared to (**ND**). Notice that the value of nonuniform fractionation is even higher under ($P2$).

The nonuniform deterministic multistage model (**ND**) is the most relaxed variant among the deterministic models. This is reflected in the fact that SDP is lowest for (**ND**) under both the settings. However, the TD (overall and OAR) for (**ND**) is higher compared to other models. The revised model (**RND**) addresses this issue and obtains solutions that are not only precise but also require lower overall radiation exposure. In this regard, (**RND**) demonstrates the desired *win-win* outcome and constitutes a collectively superior approach. Finally, when the weights are chosen to incentivize avoiding tumor underdosing ($P2$), TUD reduces for all the models studied (compare the TUD columns under the two settings). It is also worthwhile to note that under ($P2$) the exposure of OAR to radiation (radiation toxicity) is also reduced while

improving precision (lower SDP). This last observation indicates the importance of considering an objective that emphasizes tumor underdosing as opposed to a symmetric precision-based objective.

As we have mentioned earlier, a popular method for comparing radiation plans is through DVHs (Pardalos & Romeijn 2009, Drzymala et al. 1991). These illustrations capture the proportion of a particular patient structure which receives more than a specified amount of dosage. Out of the twelve instances, we present DVHs across the two parameter settings ($P1$ and $P2$) for Scan Sequence 1. From the two collections of DVH Figures 1 and 2, we determine that for this scan sequence, the static model is "fortunate" and provides comparable results for the femur structures (1(c),1(d), 2(c),2(d)). On the other hand, the DVHs show the static model is exposing the patient's bladder to infeasible amounts of radiation (1(b), 2(b)). This observation accompanied with the numerical results summarized above indicate the need to reevaluate the use of static approach for RTP. In regards to the other three multistage models, the illustrations are much more analogous across the varying structures, weights, and performance metrics. Overall, the visual comparison is in accordance with the results from the numerical output.

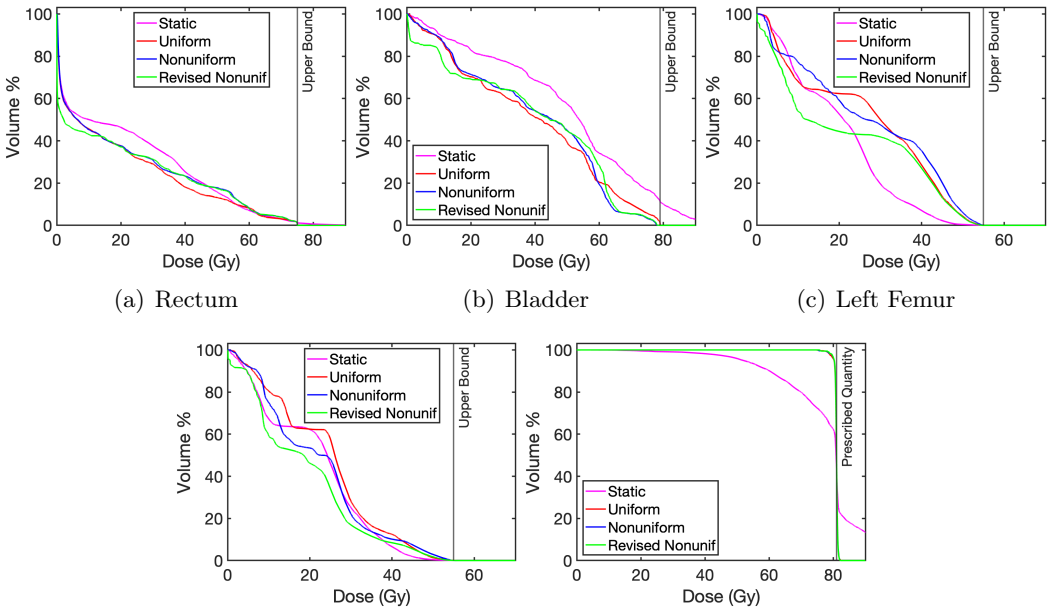


(a) Rectum (b) Bladder (c) Left Femur

(d) Right Femur (e) Tumor

Figure 1: An Illustrative Comparison of OAR and Prostate Tumor DVHs for Deterministic Models under Scan Sequence 1 (Scans 1,4,3) and Parameter Set $P1$.

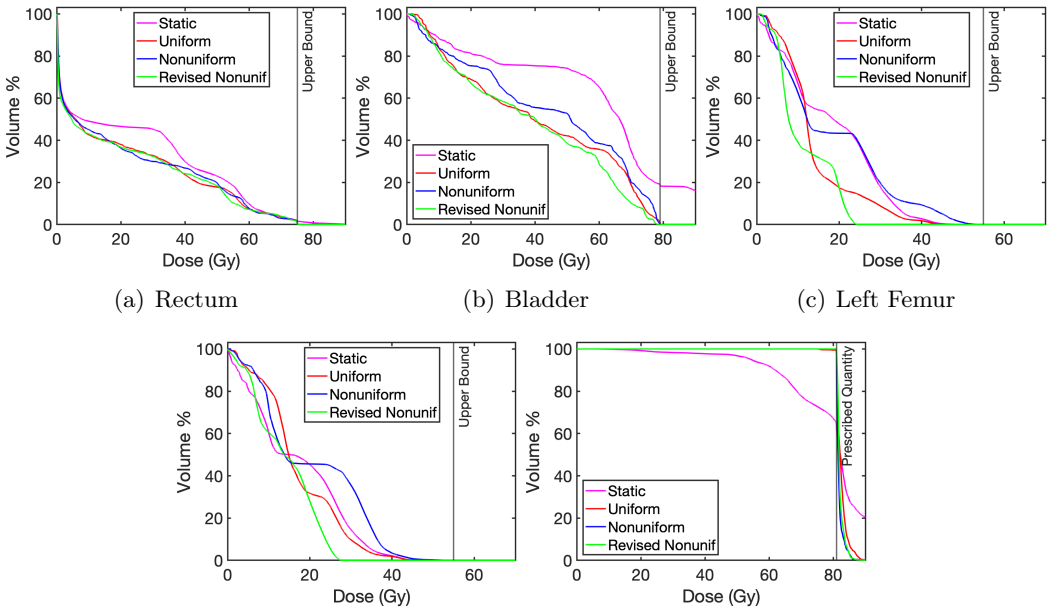


(a) Rectum (b) Bladder (c) Left Femur

(d) Right Femur (e) Tumor

Figure 2: An Illustrative Comparison of OAR and Prostate Tumor DVHs for Deterministic Models under Scan Sequence 1 (Scans 1,4,3) and Parameter Set $P2$.

### 3.3.2 Impact of the Degree of Nonuniformity

While the nonuniform fractionation models (**ND**) and (**RND**) provide flexibility in choosing the fraction-specific dose prescriptions, the resulting values for $\ell_n$ and $\mathbf{z}_n$ may deviate significantly between fractions. For example, (**RND**) assigns a tumor dose schedule of $\ell_n = (10.39, 30.00, 40.61)$ for $n = 1, 2, 3$ in one case of our numerical experiment. Such drastic variation between fractions is clinically undesirable, and, hence, in the next set of experiments, we explore the impact of varying the degree of nonuniformity in fractionation.

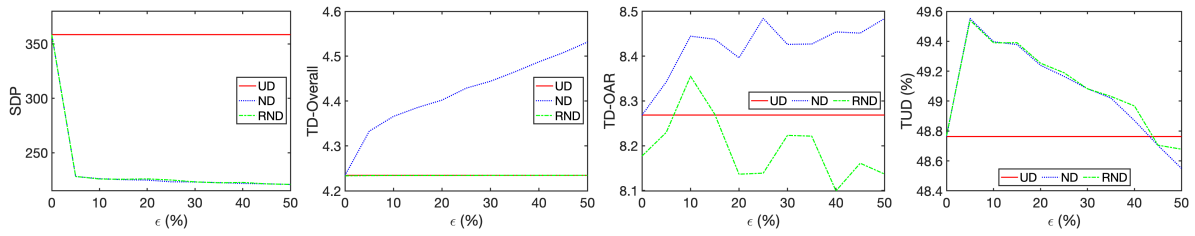


(a) SDP (b) TD-Overall (c) TD-OAR (d) TUD

Figure 3: An Evaluation of Deterministic Models' Performance across Metrics of Interest for Varying Degrees of Nonuniformity ($\epsilon \in [0, 0.50]$) under Parameter Set $P1$.

Recall that the degree of nonuniformity is determined by the value of $\epsilon \in [0, M]$ used in the

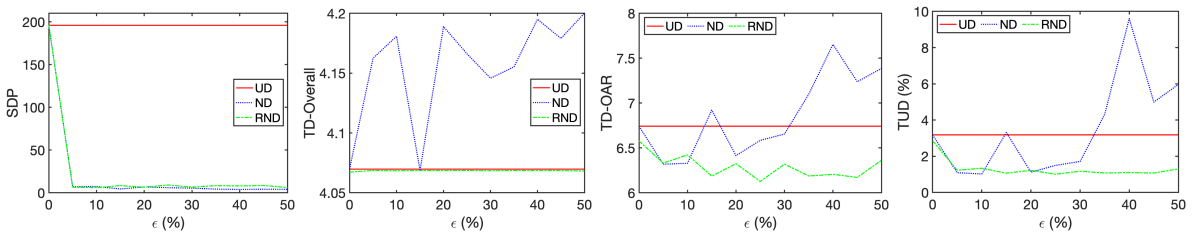


(a) SDP (b) TD-Overall (c) TD-OAR (d) TUD

Figure 4: An Evaluation of Deterministic Models' Performance across Metrics of Interest for Varying Degrees of Nonuniformity ($\epsilon \in [0, 0.50]$) under Parameter Set $P2$.

description of the set $\mathcal{U}_n^\epsilon$ for any $n$. While $\epsilon = M$ results in the highest degree of nonuniformity, a value of $\epsilon = 0$ implies a uniform fractionation scheme. We keep all the other parameters in $P1$ and $P2$ the same while varying $\epsilon$ between 0.05 to 0.50. This implies that if we were to restrict (**ND**) or (**RND**) to, say 10% nonuniformity, the fraction-specific tumor prescriptions for each fraction must be within $[24.3, 29.7]$.

Figures 3 and 4 present the overall trend of SDP, TD-Overall, TD-OAR, and TUD for (**UD**), (**ND**), and (**RND**) as we vary the degree of nonuniformity. The (**RND**) outperforms the other models in terms of SDP. Moreover, there is only a limited variation in SDP when the value of $\epsilon$ is increased. It is worthwhile to note that even when only 5% of deviation is allowed, we observe significant improvement in SDP under both the parameter settings. The results also indicate that the performance of (**RND**) is comparable to that of (**ND**), measured in terms of SDP. On the other hand, the revised model outperforms other models in terms of TD-OAR and TUD.

The deterministic multistage models utilize a perfect prediction of future evolution. However, one should expect the presence of errors in such predictions. Motivated by the performance of the multistage models in deterministic settings, we next present stochastic multistage models. These stochastic models utilize a certain representation of the future evolution that accounts for prediction errors. This extension brings forth a practical approach that requires the departure from a deterministic optimization toward stochastic optimization methods.

# 4 Stochastic Multistage Formulations

There are two possible sources of stochasticity encountered during radiation therapy (Romeijn & Dempsey 2008, Men et al. 2012, Bortfeld et al. 2006, Yan & Lockman 2001, Rietzel et al. 2005). The first source pertains to treatment geometry that includes errors in setting up the patient on the treatment device and errors resulting from breathing and peristaltic movements. We refer to such sources of stochasticity as intrafractional uncertainty. The second source is the interfractional uncertainty which includes the evolution of structures throughout the treatment. Previous work on optimization-based RTP models that explicitly accommodate stochasticity can be classified as robust optimization models (e.g., Chu et al. (2005), Chan et al. (2006), Unkelbach et al. (2018)), risk-based optimization models (Lim et al. 2020, Zaghian et al. 2018, An et al. 2017), or risk-neutral stochastic programming models (Men et al. 2012, Sir et al. 2012).

The models we present in this section have potential to accommodate interfractional uncertainty in the form of a patient's structural volume evolution as well as uncertainties associated with future predictions. Similar to Section 3, we begin by first presenting the uniform stochastic multistage formulation. Afterward, we present the revised nonuniform stochastic formulation. In the stochastic models, we aim to minimize the expected value of SDP computed across all $N$ fractions. Using the same robust approaches as intrafractional settings results in overtly conservative decisions when multiple stages are involved. Therefore, we adopt multistage models that utilize a scenario tree representation of uncertainty.

In the stochastic multistage setting, as in the case of the deterministic setting, we know the patient's current condition from the latest CT scan. However, unlike the deterministic setting where only a single prediction of structure evolution is utilized, the stochastic models explicitly account for errors in predictions. With numerical computations in mind, we depict the possible sequence of patient states in a form of a scenario tree (Shapiro et al. 2014) (see Figure 5) as explained next.

A scenario tree can be viewed as a discretization of the underlying stochastic process $\{\tilde{\xi}\}$

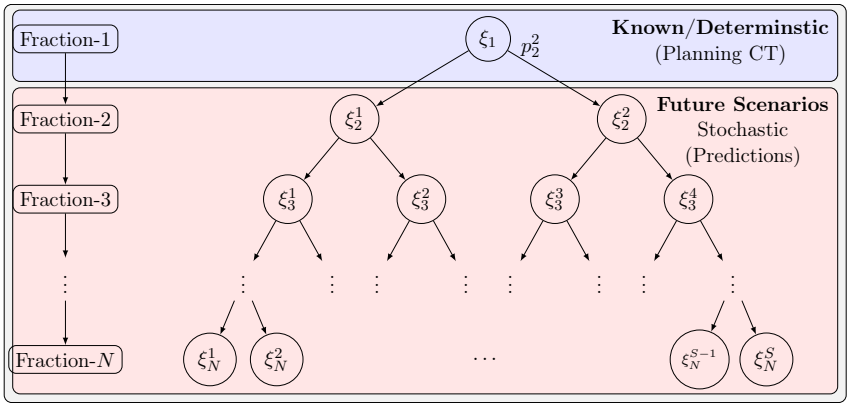


Figure 5: A Generic Scenario Tree Representation

associated with the patient's structural evolution using a set of nodes $\mathcal{J}$. The tree is arranged in stages corresponding to each fraction. The first node of the tree, also known as the root node, corresponds to the current state ($\xi_1$) and nodes in subsequent stages ($n = 2, \ldots, N$) represent possible alternative states in the corresponding fraction. For example, $\xi_3^1, \xi_3^2, \xi_3^3$, and $\xi_3^4$ represent four alternative states during Fraction 3 as shown in Figure 5. The scenario tree captures the precedence relationships (dependencies) between states in one fraction to those in the next fraction. The scenario tree also encodes $p_n^{(j)}$ as the probability of encountering node $j \in \mathcal{J}$ in fraction $n = 1, \ldots, N$.

The sequence of nodes, starting from the root node to a leaf node, is referred to as a *scenario* or a sample path. A scenario, therefore, represents a possible path of structural evolution starting from the current state of the patient. We denote the set of all possible scenarios by the set $\mathcal{K}$ and use the notation $j \in [k]$ to denote that the node $j \in \mathcal{J}$ belongs to scenario $k \in \mathcal{K}$. Notice that the number of scenarios represented on a tree is equal to the number of leaf nodes.

### 4.1 Uniform Stochastic Multistage Model

The uniform stochastic multistage model (the analog of (**UD**)) is presented in the following nested form:

$$\min \; f_1(\mathbf{x}_1, \ell_1) + \mathbb{E}_{|\xi_{[1]}}\Big[\min f_2(\mathbf{x}_2, \ell_2) + \cdots + \mathbb{E}_{|\xi_{[N-1]}}\Big[\min f_N(\mathbf{x}_N, \ell_N)\Big]\Big] \qquad (\mathbf{US})$$

$$\text{subject to } (\mathbf{x}_n, \mathbf{y}_n, \mathbf{z}_n, \ell_n) \in \mathcal{S}_n(\tilde{\xi}_n) \cap \mathcal{U}_n^0, \quad \forall n = 1, \ldots, N, \; a.s.$$

In the nested form, the expectations are taken with respect to future uncertainty conditional on information that is already realized, i.e., $\xi_{[n]} := \{\xi_i \mid i = 1, \ldots, n\}$.

When a scenario tree representation is used, the expectations can be replaced by summation over all the nodes in a given stage of the scenario tree. By duplicating the decision variables for each node, the stochastic program can be stated as a single large optimization problem known as the extensive scenario form. We refer the reader to stochastic programming textbooks Birge & Louveaux (2011), Shapiro et al. (2014) for more details on how to construct such extensive scenario forms. Consequently, the optimal solution of a stochastic multistage model will provide FMs for all the nodes in a scenario tree. The FM corresponding to the root node $(\mathbf{x}_1^\star, \mathbf{y}_1^\star)$ is recommended for treating in the first fraction. The FMs $(\mathbf{x}_n^{j,\star}, \mathbf{y}_n^{j,\star})$ for the nodes $j \in \mathcal{J}$ in future stages $(n = 2, \ldots, N)$ are advisory in nature, with a possibility of updating them in the future.

As is the case in deterministic uniform fractionation, the stochastic uniform fractionation model in (**US**) also decomposes into smaller optimization problems. In the case of (**US**), this decomposition is by nodes in the scenario tree. This feature is captured in the following result.

**Proposition 4.1.** *Under a uniform fractionation scheme,* (**US**) *decomposes into a collection of individual FM optimization problems corresponding to nodes $j \in \mathcal{J}$ in the scenario tree. That is,* (**US**) *is equivalent to*

$$\sum_{j \in \mathcal{J}} p_n^j \min \left\{ f_n(\mathbf{x}_n, \ell_n) \mid (\mathbf{x}_n, \mathbf{y}_n, \mathbf{z}_n, \ell_n) \in \mathcal{S}_n(\xi_n^j) \cap \mathcal{U}_n^0 \right\}.$$

*Proof.* Since $(\mathbf{z}_n, \ell_n) \in \mathcal{U}_n^0$, we have that fraction-specific dose prescriptions satisfy $\ell_n = \frac{L^{\text{tumor}}}{N}$ and $z_n^{(i)} = \frac{u^{(i)}}{N}$ for all $i \in \mathcal{O}$ (see (2)). Consequently, we can project the set $\mathcal{S}_n(\xi_n^j)$ to a linear subspace where the FM decisions $(\mathbf{x}_n, \mathbf{y}_n)$ satisfy (3) and (4). Since constraints (3) and (1b) are specific to a realization in a fraction (for $z_n^{(i)} = \frac{u^{(i)}}{N}$ $\forall i \in \mathcal{O}$), the optimization problem decomposes by nodes in the scenario tree. Therefore, the expectation-valued objective function can be written as the sum of node-specific objective function that are weighted by the probability of encountering the node. □

The above result illustrates that the value of lookahead information (either stochastic or deterministic) is zero when uniform fractionation scheme is adopted. Therefore, if the clinical practice forbids the adoption of nonuniform fractionation, then solving a fraction-specific optimization problem that only uses current CT scan information ($\xi_1$) will suffice.

### 4.2 Nonuniform Stochastic Multistage Model

Similar to the deterministic setting, we relax the fractionation scheme and allow the optimization model to determine fraction-specific dose prescriptions. However, a nonuniform model may provide a precise approach that results in an ideal SDP but drastically higher TD (Overall and OAR), as was observed in the numerical experiments with deterministic models (see Section 3.3). Given that we strive to obtain *win-win* outcomes when comparing TD (Overall and OAR) and SDP, the AD quantities obtained from solving (**US**) are utilized to bound the corresponding quantities in the nonuniform model. Unlike the deterministic setting where we have a single prediction, in the stochastic setting, we have multiple scenarios. To develop a suitable bound, we define the realized AD along a scenario $k \in \mathcal{K}$ as

$$\tau(k) = \sum_{n=1}^{N} \sum_{i \in \mathcal{T}} \sum_{v \in \mathcal{V}_n^{(i)}} \sum_{j \in \mathcal{J}} \mathbb{1}_{j \in [k]} x_{vn}^j, \tag{9}$$

where $\mathbb{1}_{(\bullet)}$ is an indicator function. When an optimal solution is used to compute the realized AD, we will denote it by $\tau^\star(k)$. Using the above, we state the nonuniform stochastic multistage problem as

$$\min \ f_1(\mathbf{x}_1, \ell_1) + \mathbb{E}_{|\xi_{[1]}} \Big[ \min f_2(\mathbf{x}_2, \ell_2) + \cdots + \mathbb{E}_{|\xi_{[N-1]}} \Big[ \min f_N(\mathbf{x}_N, \ell_N) \Big] \Big] \qquad (\mathbf{RNS})$$

$$\text{subject to (1)}; \ (\mathbf{x}_n, \mathbf{y}_n, \mathbf{z}_n, \ell_n) \in \mathcal{S}_n(\tilde{\xi}_n) \cap \mathcal{U}_n^\epsilon, \qquad \forall n = 1, \ldots, N, \ a.s.,$$

$$\sum_{n=1}^{N} \sum_{i \in \mathcal{T}} \sum_{v \in \mathcal{V}_n^{(i)}} x_{vn} \leq \tau(k) \qquad \forall k \in \mathcal{K}.$$

The above model determines the fraction-specific dose prescriptions and FMs that are hedged against the possible errors in predicting the evolution of the structures in the future. The second constraint ensures that the AD prescribed by (**RNS**) is within an upper bound given by $\tau(k)$ for each scenario $k \in \mathcal{K}$. Similar to (**RND**), we use upper bounds computed from the optimal

solution of (**US**).

**Procedure 2** Nonuniform Stochastic Fractionation

1: **Input:** Number of fractions, $N$; dose prescription specifying $\mathbf{u}$ and $L^{\text{tumor}}$; current CT-scan information $\xi_1$; a scenario tree representing possible scenarios of structural evolution $\{\xi_n^j\}_{n=2}^N$ and $j \in \mathcal{J}$.

2: Compute the dose-deposition matrices $\mathbf{A}_n^i$ for all nodes on a scenario tree ($n = 1, \ldots, N$, $j \in \mathcal{J}$).

3: Solve the uniform stochastic model (**US**) and obtain the optimal solution $\mathbf{x}_n^{\star US}$ for $n = 1, \ldots, N$ and $j \in \mathcal{J}$.

4: Compute the AD $\tau(k)$ for all $k \in \mathcal{K}$.

5: Instantiate and solve the revised nonuniform model (**RNS**). Obtain the optimal solution.

6: **Output:** The optimal dose prescriptions $(\mathbf{z}_1^\star, \ell_1^\star)$ and the beamlet intensities $\mathbf{y}_1^\star$.

In the presence of prediction errors, we adopt Procedure 2 under a nonuniform fractionation scheme. Following Proposition 4.1, in Step 3, we can solve the uniform node-specific FM optimization problem for each node of the scenario tree. We next turn to numerical experimentation in order to draw comparison between (**US**) and (**RNS**).

### 4.3 Numerical Results Comparing Stochastic Models

Again using the CT scan data provided by Saberian & Kim (2014), we conduct numerical experiments with the stochastic multistage models to achieve the following two objectives. First, we quantify the value of nonuniform fractionation in a stochastic problem setting. Second, we establish the value of a stochastic solution when compared to the potential approaches that ignore uncertainty entirely.

For the case where $N = 3$, we consider the scan sequences summarized in Table 4 resulting in four distinct scenario trees labeled ST1, ST2, ST3, and ST4. We set the conditional probabilities at all non-terminal nodes to 0.5. Generating the collection of scenario trees requires assigning

a variety of combinations of nodes at each stage. Table 4 outlines the composition of each of

| Scenario Tree | First-Stage Node | Second-Stage Nodes | Third-Stage Nodes |
|---|---|---|---|
| ST1 | Scan 2 | Scans 1,4 | Scans 5,3 |
| ST2 | Scan 1 | Scans 2,5 | Scans 3,4 |
| ST3 | Scan 4 | Scans 2,3 | Scans 1,5 |
| ST4 | Scan 5 | Scans 1,3 | Scans 2,4 |

Table 4: Scan Sequences Used to Generate Scenario Trees for Stochastic Multistage Models.

the four scenario trees considered. All scenario trees have a fixed first-stage scan, two second-stage nodes (predictions), and two third-stage nodes (predictions) which provide four unique scenarios per tree. Instances of the stochastic multistage models (**US**) and (**RNS**) are generated and solved for ST1, ST2, ST3, and ST4. We note that determining the appropriate number of prediction scenarios, or equivalently the number nodes at each stage of the scenario tree, is non-trivial and requires further research. While we consider only two nodes at each stage for the sake of demonstration, we emphasize that the proposed stochastic programming methodology can incorporate a large number of scenarios. We report the complete results for all the metrics described in Section 2.2.

#### 4.3.1 A Comparison of the Metrics of Interest under Stochastic Models

Table 5 summarizes the comprehensive numerical results of stochastic multistage models (**US**) and (**RNS**). We report the average, standard deviation (std. dev.), and range of the metrics of interest computed across all numerical instances, i.e, for all of the scenario trees (ST1, ST2, ST3, and ST4) under $P1$ and $P2$. For (**RNS**), we also present the percentage improvement in the average values of metrics relative to the results obtained from (**US**) computed.

In support of the results provided in Table 5, a pairwise t-test was conducted to determine the existence of statistically significant differences between the objective function values of the two stochastic models, i.e., SDP values of (**US**) versus (**RNS**). The null hypothesis of the pairwise t-test conducted is that the mean of the paired differences of the SDP values under (**US**) and (**RNS**) equals zero over all the scenario trees considered in our experiments. That is, the null hypothesis is that the two models yield statistically similar results. Examination of

the findings reveals the clear advantages of (**RNS**). In terms of parameter set $P1$, the resulting test statistic and corresponding p-value are 2.0440 and 0.1335, respectively. For the parameter set $P2$, however, the statistical comparison yields a test statistic of 5.5971 and a p-value 0.0113. Hence, there exists a significant difference ($p < 0.05$) between the two models and the superior performance of (**RNS**) is more notable in the context of parameter set $P2$.

To further illustrate the comparison between (**US**) and (**RNS**), we present the box-and-whisker plots in Figures 6 generated using results from Table 5. In a box-and-whisker plot, the top and bottom of the box represents the $75^{th}$ and $25^{th}$ quantiles, respectively, whereas the central red line indicates the median and the whiskers are the extreme values. The results reveal the significant improvement in terms of SDP in (**RNS**) for both parameter sets $P1$ and $P2$. Notice that the minimum SDP obtained from (**US**) is higher than the maximum

| Parameter Set $P1$ | | | | | |
|---|---|---|---|---|---|
| | | SDP | TD-Overall | TD-OAR | TUD |
| (**US**) | Average | 372.4063 | 4.0439 | 8.4727 | 47.8338 |
| | Std. dev. | 29.0147 | 0.1546 | 0.2489 | 0.1153 |
| | Range | [347.7997 , 411.0633] | [3.8792 , 4.2293] | [8.3057 , 8.8420] | [47.7138 , 47.9886] |
| (**RNS**) | Average | 331.6761 | 4.0409 | 8.1663 | 47.6843 |
| | Std. dev. | 12.0001 | 0.1550 | 0.5814 | 0.3375 |
| | Range | [313.8627 , 339.6415] | [3.8776 , 4.2280] | [7.6308 , 8.9219] | [47.2869 , 48.0817] |
| | Improve (%) | 10.9370 | 0.0742 | 3.6163 | 0.3125 |
| Parameter Set $P2$ | | | | | |
| | | SDP | TD-Overall | TD-OAR | TUD |
| (**US**) | Average | 157.3246 | 3.8332 | 7.2790 | 3.8876 |
| | Std. dev. | 44.9074 | 0.1451 | 0.1982 | 0.3612 |
| | Range | [127.0373 , 222.1330] | [3.6510 , 4.0008] | [7.0889 , 7.5428] | [3.6562 , 4.4180] |
| (**RNS**) | Average | 23.2651 | 3.8305 | 6.3381 | 1.4558 |
| | Std. dev. | 3.1202 | 0.1455 | 0.2426 | 0.5875 |
| | Range | [18.6973 , 25.7280] | [3.6483 , 4.9991] | [6.1182 , 6.5973] | [0.9338 , 2.1868] |
| | Improve (%) | 85.2120 | 0.0704 | 12.9262 | 62.8100 |

Table 5: A Comparison of Metrics of Interest for Stochastic Multistage Models under Parameter Sets $P1$ and $P2$: Comprehensive Numerical Results Reporting Average Values, Standard Deviations, and Ranges over All Numerical Instances.

SDP obtained from (**RNS**), indicating that the nonuniform fractionation scheme dominates the uniform fractionation scheme across all the representations of uncertainty considered in our experiment. The dominance is much more significant for $P2$ when compared to $P1$. The two fractionation schemes are not distinguishable in terms TD-Overall under both settings. There is a noticeable increase in the variance of TD-OAR and TUD metrics under $P1$ (observe the increased box widths). On the other hand, the domination of the nonuniform fractionation across all uncertainty representations is seen in the box plots associated with TD-OAR and TUD.

We further illustrate the differences between the uniform and nonuniform fractionation schemes by analyzing their performance across individual scenarios of a representative scenario tree, ST1. We begin by instantiating the multistage models for ST1, solve the resulting optimization problem to optimality, and compute the metrics of interest along each scenario of ST1. We present in Table 6 the results of this analysis for both parameter settings $P1$ and $P2$. For (**US**), the table shows the metrics for each of the four scenarios in ST1. On the other hand, for (**RNS**), the table shows the metrics along with the relative difference (in %) between the results

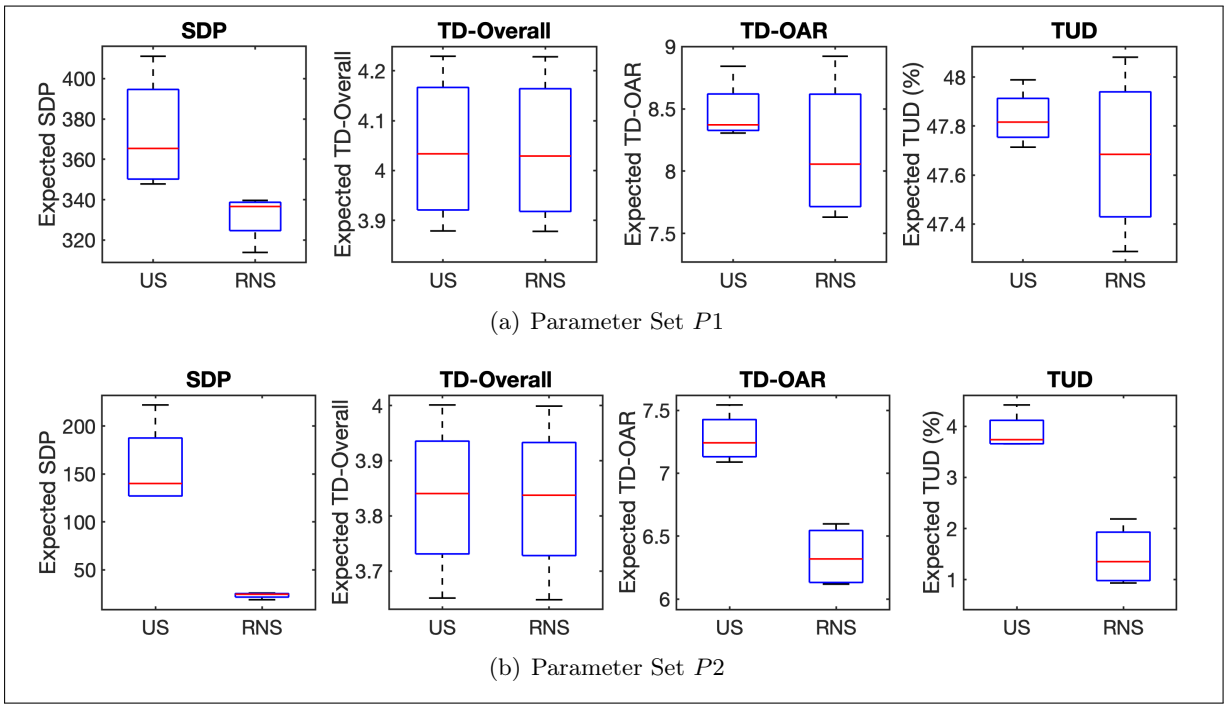


(a) Parameter Set $P1$

(b) Parameter Set $P2$

Figure 6: A Comprehensive Boxplot Comparison of Metrics of Interest for Stochastic Multistage Models under Parameter Sets $P1$ and $P2$.

obtained from (**RNS**) and (**US**). A positive (or a negative) difference indicates an improvement (or a deterioration) in performance from (**RNS**), when compared to (**US**). It is worthwhile to note that, as a consequence of observation in (7) and Proposition 4.1, the scenario-specific results for (**US**) in Table 6 are equivalent to the uniform deterministic fractionation (Procedure 1) applied to the corresponding scenario.

| Parameter Set $P1$ | | | | | |
|---|---|---|---|---|---|
| | Scenario | SDP | TD-Overall | TD-OAR | TUD |
| (**US**) | 1 | 462.8094 | 4.2105 | 8.4619 | 47.2232 |
| | 2 | 410.4636 | 3.9936 | 8.0620 | 48.8396 |
| | 3 | 345.8717 | 3.7215 | 8.5621 | 46.8360 |
| | 4 | 293.5260 | 3.5914 | 8.1370 | 48.4524 |
| (**RNS**) | 1 | 407.3993 (11.97%) | 4.2084 (0.05%) | 8.4942 (−0.38%) | 47.0804 (0.30%) |
| | 2 | 272.1991 (33.69%) | 3.9936 (0.00%) | 7.9351 (1.57%) | 48.6540 (0.38%) |
| | 3 | 355.5262 (−2.79%) | 3.7183 (0.08%) | 8.7129 (−1.76%) | 46.4871 (0.75%) |
| | 4 | 220.3260 (24.94%) | 3.5901 (0.04%) | 8.1116 (0.31%) | 48.0606 (0.81%) |
| Parameter Set $P2$ | | | | | |
| | Scenario | SDP | TD-Overall | TD-OAR | TUD |
| (**US**) | 1 | 248.6650 | 3.9054 | 7.9473 | 4.9415 |
| | 2 | 247.5025 | 3.6895 | 7.5614 | 4.2037 |
| | 3 | 58.5761 | 3.5777 | 7.5132 | 3.4274 |
| | 4 | 57.4136 | 3.4314 | 7.1494 | 2.6896 |
| (**RNS**) | 1 | 24.0225 (90.34%) | 3.9009 (0.11%) | 6.3303 (20.35%) | 1.6219 (67.18%) |
| | 2 | 14.6681 (94.07%) | 3.6864 (0.08%) | 6.7227 (11.09%) | 0.7182 (82.91%) |
| | 3 | 22.7265 (61.20%) | 3.5755 (0.06%) | 5.4679 (27.22%) | 1.3414 (60.86%) |
| | 4 | 13.3720 (76.71%) | 3.4302 (0.04%) | 5.9519 (16.75%) | 0.4378 (83.72%) |

Table 6: An Illustrative Comparison of Metrics of Interest for Stochastic Multistage Models Across Each Individual Scenario of Scenario Tree ST1 under Parameter Sets $P1$ and $P2$.

The results in Table 6 show that (**RNS**) dominates the uniform approach across all metrics for every realizable scenario under parameter set $P2$. However, this is not the case for the equally weighted setup of ($P1$). Table 6 reveals that although the uniform deterministic approach outperforms the nonuniform stochastic approach for certain scenarios (e.g., Scenario 3 for $P1$), it is impossible to identify such scenarios a priori. When (**US**) dominates (**RNS**), the magnitude

tends to be less significant than when (**RNS**) outperforms (**US**). As is the case in comprehensive results (Table 5 and Figure 6), the advantages of nonuniform fractionation are more pronounced in setting $P2$, specifically with respect to metrics SDP, TD-OAR, and TUD. There is only marginal improvement in terms of TD-Overall.

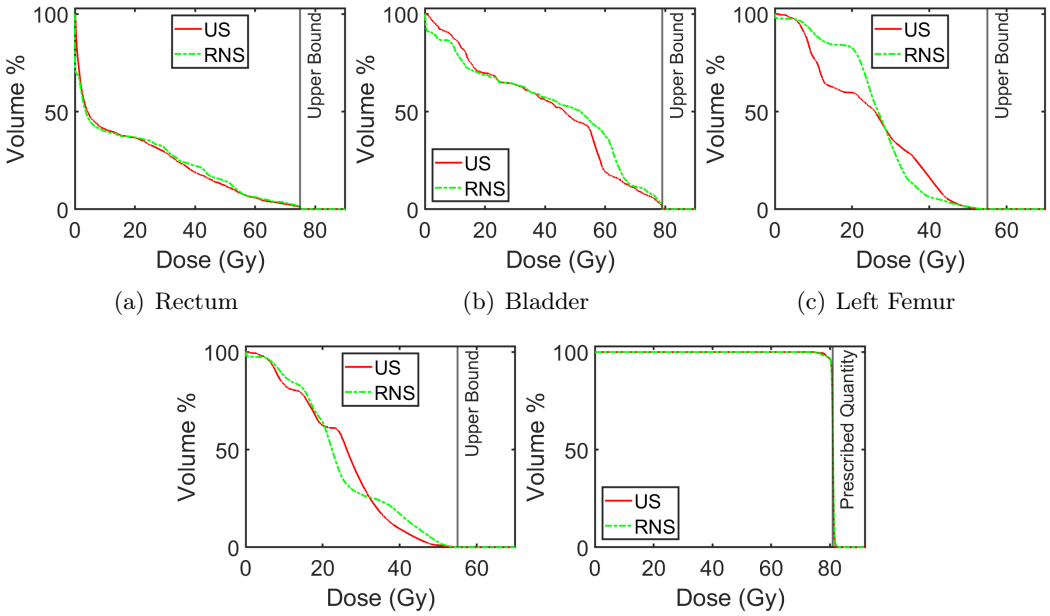


(a) Rectum (b) Bladder (c) Left Femur

(d) Right Femur (e) Tumor

Figure 7: An Illustrative Comparison of OAR and Prostate Tumor DVHs for Stochastic Multi-stage Models under Scenario 2 (Scans 2,1,3) of Scenario Tree ST1 and Parameter Set $P1$.

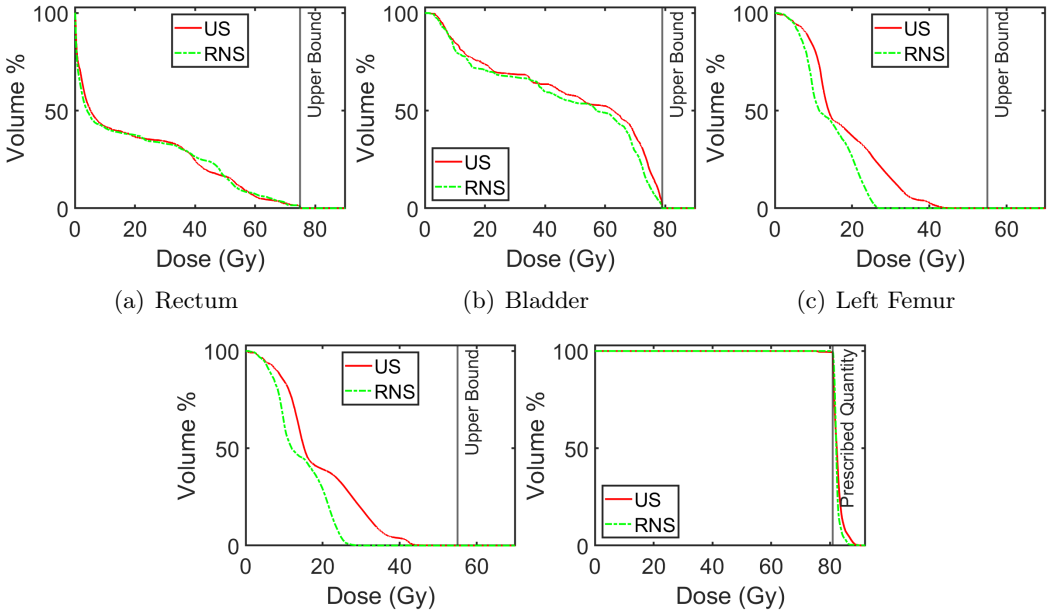


(a) Rectum (b) Bladder (c) Left Femur

(d) Right Femur (e) Tumor

Figure 8: An Illustrative Comparison of OAR and Prostate Tumor DVHs for Stochastic Multi-stage Models under Scenario 2 (Scans 2,1,3) of Scenario Tree ST1 and Parameter Set $P2$.

### 4.3.2 An Illustrative Examination of DVHs under Stochastic Models

To provide an illustrative comparison to complement the scenario-based results in Table 6, we generate the DVHs corresponding to Scenario 2 of ST1 across both parameter sets $P1$ and $P2$. Here, Scenario 2 was chosen with the intention of providing DVHs that demonstrate conclusive takeaways in regards to the comparison between (**US**) and (**RNS**). However, as demonstrated in Table 6, Scenario 2 under $P1$ represents negligible differences between the performance of (**US**) and (**RNS**) across all four metrics. When Scenario 2 is considered under $P2$, the results in Table 6 give (**RNS**) a convincing advantage over (**US**). Collectively, the illustrative DVH comparisons align with the numerical output corresponding to Scenario 2 in Table 6.

The numerical results summarized in Table 6 along with the DVHs in Figures 7 and 8 also illustrate and support the necessity to consider nonuniform fractionation schemes in a stochastic problem setting. Although (**US**) is dominated in performance when compared with (**RNS**) under $P2$, both of these approaches are capable of providing valuable advantages over models which ignore uncertainty completely.

## 5 Conclusion

The commonly practiced uniform fractionation approach to RTP cannot accommodate lookahead information or use predictive analytics tools to incorporate tumor evolution information for planning. In an attempt to remedy this shortcoming, we propose new modeling approaches that enable a superior representation of multistage RTP problems by explicitly incorporating uncertainty as well as allowing a nonuniform fractionation scheme. Utilizing lookahead information explicitly to consider uncertainty in future evolution of the tumor, our nonuniform fractionation models result in dose prescriptions and FMs that are adaptable and responsive to the interfractional evolution of the patient's state and condition.

We demonstrate that our approach can drastically improve the quality of treatment plans in terms of multiple metrics of interest. The improvements are maintained even when we restrict

the underlying fractionation scheme to small intervals of nonuniformity. Hence, we argue that leveraging the stochastic programming methodology, accompanied with well-developed future patient CT scan predictions, has significant promise as a resource for RTP.

We offer promising numerical results demonstrating the value of our proposed approach in terms of multiple metrics of interest. While these results provide strong motivation to consider the proposed approach for clinical implementation, there remains a need for methodological research to achieve scalability for problems with a large number of fractions. Further, the incorporation of determining an appropriate number of prediction scenarios while balancing computational expense and clinical objectives requires additional attention. Also, our initial analysis of improvements are based on numerical metrics of interest that are computable in an optimization framework, e.g., SDP, TD-Overall, TD-OAR, and TUD. Hence, there is also a need to perform a similar analysis considering clinical criteria representative of delivery accuracy of predicted FMs, such as gamma analysis and modulation complexity score. However, we note that the proposed scheme will only affect the prescription dose at each treatment fraction. It will not affect the delivery accuracy since currently available inverse planning techniques can be readily employed. Similarly, existing independent tools could be used to check the plan generated by the proposed scheme by incorporating scaling factors that reflect doses prescribed at different fractions.

The intention of this work was to demonstrate the value in nonuniform stochastic multistage models accompanied with stochastic programming solution methodology for general types of cancer requiring radiation treatment. Therefore, the implementation for various sequences of prostate cancer patient CT-scans provided one such demonstration. For clinical purposes and a specified form of cancer, the models presented in the current work would likely need to add additional OAR constraints beyond maximum dose upper bound limitations. For prostate cancer specifically, additional consideration could be given to dose accumulation and related problems as well as the differences in rectal and bladder filling and the overall prostate position relative to the rectum and bladder.

Finally, the incorporation of clinically relevant and biologically-related concepts, e.g. see Gaddy et al. (2018), into our proposed RTP models would expand the exclusive physical-criteria classification of the current work. With the intention of developing optimization tools that are eventually capable of utilization in a clinical setting, integration of the features mentioned above to the current work remains a promising future research direction.

With technological and computational advancements, we expect that the multistage stochastic programming methodologies will continue to serve as resourceful optimization tools for RTP applications. Practitioners and cancer patients in the future will hopefully benefit from the utilization of these resources. Hence, further exploration of applying stochastic programming methodologies powered by predictive analytics tools to improve RTP practices under uncertainty remains a fruitful research direction.

## References


Ahunbay, E. E., Peng, C., Chen, G., Narayanan, S., Yu, C., Lawton, C. & Li, X. A. (2008), 'An on-line replanning scheme for interfractional variations', *Medical Physics* **35**(8), 3607–3615.

An, Y., Liang, J., Schild, S. E., Bues, M. & Liu, W. (2017), 'Robust treatment planning with conditional value at risk chance constraints in intensity-modulated proton therapy', *Medical Physics* **44**(1), 28–36.

Baskar, R., Lee, K. A., Yeo, R. & Yeoh, K.-W. (2012), 'Cancer and radiation therapy: Current advances and future directions', *International Journal of Medical Sciences* **9**(3), 193–199.

Birge, J. R. & Louveaux, F. (2011), *Introduction to Stochastic Programming*, Springer.

Bortfeld, T. (1999), Optimized planning using physical objectives and constraints, *in* 'Seminars in Radiation Oncology', Vol. 9, Elsevier, pp. 20–34.

Bortfeld, T. (2006), 'IMRT: A review and preview', *Physics in Medicine & Biology* **51**(13), R363–R379.

Bortfeld, T., Neve, W., Schmidt-Ullrich, R. & Wazer, D. E. (2006), *Image-Guided IMRT*, Springer.

Brahme, A., Roos, J.-E. & Lax, I. (1982), 'Solution of an integral equation encountered in rotation therapy', *Physics in Medicine & Biology* **27**(10), 1221–1229.

Chan, T. C., Bortfeld, T. & Tsitsiklis, J. N. (2006), 'A robust approach to IMRT optimization', *Physics in Medicine & Biology* **51**(10), 2567–2583.

Chu, M., Zinchenko, Y., Henderson, S. G. & Sharpe, M. B. (2005), 'Robust optimization for intensity modulated radiation therapy treatment planning under uncertainty', *Physics in Medicine & Biology* **50**(23), 5463–5477.

Drzymala, R., Mohan, R., Brewster, L., Chu, J., Goitein, M., Harms, W. & Urie, M. (1991), 'Dose-volume histograms', *International Journal of Radiation Oncology - Biology - Physics* **21**(1), 71–78.

Ehrgott, M., Güler, Ç., Hamacher, H. W. & Shao, L. (2010), 'Mathematical optimization in intensity modulated radiation therapy', *Annals of Operations Research* **175**(1), 309–365.

Ferris, M. C. & Voelker, M. M. (2004), 'Fractionation in radiation treatment planning', *Mathematical Programming* **101**(2), 387–413.

Gaddy, M. R., Yıldız, S., Unkelbach, J. & Papp, D. (2018), 'Optimization of spatiotemporally fractionated radiotherapy treatments with bounds on the achievable benefit', *Physics in Medicine & Biology* **63**(1), 015036.

Ghate, A. (2011), Dynamic optimization in radiotherapy, *in* 'INFORMS TutORials in Operations Research: Transforming Research into Action', INFORMS, pp. 60–74.

Holder, A. & Salter, B. (2005), A tutorial on radiation oncology and optimization, *in* 'Tutorials on Emerging Methodologies and Applications in Operations Research', Springer, pp. 4:1–4:47.

Lim, G. J., Kardar, L., Ebrahimi, S. & Cao, W. (2020), 'A risk-based modeling approach for

radiation therapy treatment planning under tumor shrinkage uncertainty', *European Journal of Operational Research* **280**(1), 266–278.

Lu, W., Chen, M., Chen, Q., Ruchala, K. & Olivera, G. (2008), 'Adaptive fractionation therapy: I. basic concept and strategy', *Physics in Medicine & Biology* **53**(19), 5495–5511.

McDonald, S. C. & Rubin, P. (1977), 'Optimization of external beam radiation therapy', *International Journal of Radiation Oncology - Biology - Physics* **2**(3-4), 307–317.

Mell, L. K., Roeske, J. C. & Mundt, A. J. (2003), 'A survey of intensity-modulated radiation therapy use in the united states', *Cancer* **98**(1), 204–211.

Men, C., Romeijn, H. E., Saito, A. & Dempsey, J. F. (2012), 'An efficient approach to incorporating interfraction motion in IMRT treatment planning', *Computers & Operations Research* **39**(7), 1779–1789.

Mills, M. D. & Woo, S. Y. (2015), History of IMRT, *in* 'Intensity-Modulated Radiation Therapy', Springer, pp. 3–14.

Oh, S. & Kim, S. (2017), 'Deformable image registration in radiation therapy', *Radiation Oncology Journal* **35**(2), 101–111.

Pardalos, P. M. & Romeijn, H. E. (2009), *Handbook of Optimization in Medicine*, Springer Science & Business Media.

Ramakrishnan, J., Craft, D., Bortfeld, T. & Tsitsiklis, J. N. (2012), 'A dynamic programming approach to adaptive fractionation', *Physics in Medicine and Biology* **57**(5), 1203–1216.

Redpath, A., Vickery, B. & Wright, D. (1976), 'A new technique for radiotherapy planning using quadratic programming', *Physics in Medicine & Biology* **21**(5), 781–791.

Rietzel, E., Chen, G. T., Choi, N. C. & Willet, C. G. (2005), 'Four-dimensional image-based treatment planning: Target volume segmentation and dose calculation in the presence of respiratory motion', *International Journal of Radiation Oncology - Biology - Physics* **61**(5), 1535–1550.

Romeijn, H. E. & Dempsey, J. F. (2008), 'Intensity modulated radiation therapy treatment plan optimization', *TOP* **16**(2), 215–243.

Saberian, F., Ghate, A. & Kim, M. (2016), 'Optimal fractionation in radiotherapy with multiple normal tissues', *Mathematical Medicine and Biology: A Journal of the IMA* **33**(2), 211–252.

Saberian, F., Ghate, A. & Kim, M. (2017), 'Spatiotemporally optimal fractionation in radiotherapy', *INFORMS Journal on Computing* **29**(3), 422–437.

Saberian, F. & Kim, M. (2014), 'Phantom creator (phanc): A matlab software for creating phantom test cases for IMRT optimization, working draft of the user's manual', *University of Washington* .

Shapiro, A., Dentcheva, D. & Ruszczynski, A. (2014), *Lectures on Stochastic Programming: Modeling and Theory*, SIAM.

Shepard, D. M., Ferris, M. C., Olivera, G. H. & Mackie, T. R. (1999), 'Optimizing the delivery of radiation therapy to cancer patients', *Siam Review* **41**(4), 721–744.

Sir, M. Y., Epelman, M. A. & Pollock, S. M. (2012), 'Stochastic programming for off-line adaptive radiotherapy', *Annals of Operations Research* **196**(1), 767–797.

Starkschall, G. (1984), 'A constrained least-squares optimization method for external beam radiation therapy treatment planning', *Medical Physics* **11**(5), 659–665.

Teh, B. S., Woo, S. Y. & Butler, E. B. (1999), 'Intensity modulated radiation therapy (IMRT): A new promising technology in radiation oncology', *The Oncologist* **4**(6), 433–442.

Unkelbach, J., Alber, M., Bangert, M., Bokrantz, R., Chan, T. C., Deasy, J. O., Fredriksson, A., Gorissen, B. L., Van Herk, M., Liu, W. et al. (2018), 'Robust radiotherapy planning', *Physics in Medicine & Biology* **63**(22), 22TR02:1–28.

Wallace, S. W. & Ziemba, W. T. (2005), *Applications of Stochastic Programming*, SIAM.

Webb, S. (2003), 'The physical basis of IMRT and inverse planning', *The British journal of radiology* **76**(910), 678–689.

Yan, D. & Lockman, D. (2001), 'Organ/patient geometric variation in external beam radiotherapy and its effects', *Medical Physics* **28**(4), 593–602.

Yan, D., Vicini, F., Wong, J. & Martinez, A. (1997), 'Adaptive radiation therapy', *Physics in Medicine & Biology* **42**(1), 123–132.

Zaghian, M., Lim, G. J. & Khabazian, A. (2018), 'A chance-constrained programming framework to handle uncertainties in radiation therapy treatment planning', *European Journal of Operational Research* **266**(2), 736–745.

# A Appendix: Summary of Essential Notation

| Sets | |
|---|---|
| $N$ | Total number of fractions in the radiation treatment plan |
| $\mathcal{T}$ | Set of all relevant patient structures |
| $\mathcal{O}$ | Set of organs-at-risk (OAR) |
| $\mathcal{V}_n^{(i)}$ | Set of all voxels $v$ belonging to structure $i$ during fraction $n$ |
| $\mathcal{B}$ | Set of all radiation beamlets |
| $\mathcal{K}$ | Set of all possible scenarios corresponding to a scenario tree |
| $\mathcal{J}$ | Set of all nodes corresponding to a scenario tree |
| $\tau$ | Upper-bound quantity imposed on aggregate dose (AD) |
| Parameters | |
| $\xi$ | Observation of the stochastic process $\tilde{\xi}$ capturing interfractional uncertainty |
| $L^{\text{tumor}}$ | Total prescribed tumor dosage (in Gy units) |
| $\mathbf{u}$ | Universal upper bounds for each OAR (in Gy units) |
| $\epsilon$ | Parameter describing freedom of nonuniformity ($\epsilon \in [0, M]$) |
| $\mathbf{A}_n$ | Dose-deposition matrix ($\lvert\mathcal{V}_n\rvert \times \lvert\mathcal{B}\rvert$) in fraction $n$ |
| $(w_n^+, w_n^-)$ | Scalar importance weights characterizing tumor dosing preferences |
| $p_n^{(j)}$ | Probability of visiting node $j$ during fraction $n$ |
| $P1$ | Parameter set with equal weights, i.e., $w_n^+ = w_n^- = 0.5$, for all fractions $n$ |
| $P2$ | Parameter set with weights $w_n^+ = 0.001, w_n^- = 0.999$ for all fractions $n$ |
| Decision Variables | |
| $z_n^{(i)}$ | Upper bound dosage for all voxels belonging to OAR $i$ during fraction $n$ |
| $\ell_n$ | Prescribed tumor dosage for fraction $n$ |
| $x_{vn}$ | Dosage given to voxel $v$ during fraction $n$ |
| $y_{bn}$ | Intensity of beamlet $b$ during fraction $n$ |